

1 Direct Exchange Mechanism for Interlayer Ions in Non-Swelling Clays

2 Luis Ruiz Pestana¹, Kedarnath Kolluri², Teresa Head-Gordon^{1,3}, Laura Nielsen Lammers^{2,4*}

3 ¹Chemical Sciences Division and ²Earth and Environmental Science Area
4 Lawrence Berkeley National Laboratory

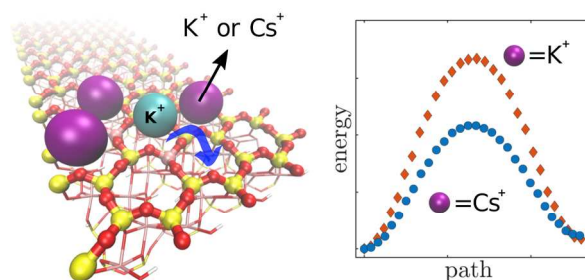
5 ³Departments of Chemistry, Bioengineering, Chemical and Biomolecular Engineering, and

6 ⁴Department of Environmental Science, Policy, and Management,
7 University of California, Berkeley

8 *Corresponding Author. Address: University of California, Berkeley, 130 Mulford Hall 3114,
9 Berkeley, CA 94720-3114. Phone: 510-664-4210. Email: lnammers@berkeley.edu

10

11 TOC figure



12

13 ABSTRACT

14 The mobility of radiocesium in the environment is largely mediated by cation exchange
15 in micaceous clays, in particular illite—a non-swelling clay mineral that naturally contains
16 interlayer K^+ and has high affinity for Cs^+ . Although exchange of interlayer K^+ for Cs^+ is
17 thermodynamically non-selective, recent experiments show that direct, anhydrous Cs^+ - K^+
18 exchange is kinetically viable and leads to the formation of phase-separated interlayers through a
19 mechanism that remains unclear. Here, using classical atomistic simulations and density
20 functional theory calculations, we identify a molecular-scale positive feedback mechanism in
21 which exchange of the larger Cs^+ for the smaller K^+ significantly lowers the migration barrier of
22 neighboring K^+ , allowing exchange to propagate rapidly once initiated at the clay edge. Barrier
23 lowering upon slight increase in layer spacing (~ 0.7 Å) during Cs^+ exchange is an example of
24 “chemical-mechanical coupling” that likely explains the observed sharp exchange fronts leading
25 to interstratification. Interestingly, we find that these features are thermodynamically favored
26 even in the absence of a heterogeneous layer charge distribution.

27

28 Keywords: clay minerals, radiocesium transport, ion exchange capacity, molecular simulation

29

30 INTRODUCTION

31 Ion exchange in layered silicate minerals mediates contaminant immobilization,¹⁻¹¹
32 weathering of micaceous minerals,¹²⁻¹⁴ and formation of interstratified nanocomposite structures
33 for engineering and petrochemical applications.¹⁵⁻¹⁸ Widespread soil radiocesium contamination
34 following the Chernobyl and Fukushima Daiichi nuclear disasters has stimulated research on
35 how micaceous minerals, which bear sites with an extremely high affinity for Cs⁺, mediate
36 radiocesium transport. The availability of these high-affinity sites will largely dictate the long-
37 term retention of soil Cs⁺, and these sites are thought to be located in the edge and interlayer
38 regions of micas and micaceous clay minerals.¹⁹ Edges have a relatively small exchange capacity,
39 with estimates ranging from ~2%²⁰ to ~20%²¹⁻²² of the total cation exchange capacity (CEC)
40 depending on particle size and solution composition. Only a fraction of these (~0.5-10%) are
41 thought to be high-affinity sites.²³ Counterions occupying interlayer regions in micaceous
42 minerals are typically considered inaccessible to exchange, severely limiting the overall
43 availability of high affinity sorption sites for long-term radiocesium immobilization.

44 Exchange of interlayer K⁺ in layered silicates has been studied for more than half a
45 century to understand mica weathering and to quantify overall ion exchange capacities of the
46 layered silicates.^{12-14, 24} The key parameters controlling the extent of anhydrous potassium ion
47 exchange (i.e. “weatherability”) include the magnitude of the layer charge, particle size, the
48 identity of the exchanger ion, and the presence of K⁺ in solution.^{12, 25} Divalent ions and small
49 monovalent ions maintain solvation complexes in the interlayer region, while large monovalent
50 ions such as K⁺, Cs⁺, and NH₄⁺ tend to be anhydrous. Exchange experiments in relatively high
51 structural charge micas and illite clays have demonstrated that replacement of anhydrous K⁺ by
52 hydrated ions of Na⁺, Ba²⁺, and Sr^{2+13, 25-28} is kinetically accessible through a hydration
53 mechanism involving significant clay layer expansion or “decollapse” typical of clay minerals
54 classified as vermiculites. Replacement of interlayer K⁺ from micas proceeds inwards from the
55 edge, often leaving behind a central core of ions inaccessible to exchange.²⁹ Nanoscale imaging
56 of the interlayer exchange process *in situ* has shown that propagation of the exchange front—the
57 interface between non-exchanged and exchanged interlayer regions—is linear in the square root
58 of time, indicating diffusion controlled exchange kinetics.²⁵ In all prior determinations of

59 interlayer exchange and diffusion kinetics, the exchanger ion has been either been hydrated,^{13,25,}
60 ^{27-28, 30} or exchange of an anhydrous ion has been mediated by prior exchange by a hydrated
61 ion.^{14, 31-32} In this case, a “collapse-decollapse” kinetic mechanism involving hydrated ion
62 intermediates was assumed to facilitate exchange of Cs⁺ in the interlayer region.³⁰ However, due
63 to strong thermodynamic penalty for replacement of K⁺ by hydrated ions in the interlayer,²⁶ the
64 presence of even trace amounts of aqueous K⁺ or NH₄⁺ strongly inhibits exchange by solvated
65 counterions,^{12, 33} making a decollapse mechanism unlikely under typical environmental
66 conditions. Thus the underlying microscopic explanation for accessibility of clay interlayers to
67 exchange with anhydrous ions such as Cs⁺ and NH₄⁺ is effectively unknown.

68 Direct exchange of anhydrous ions in collapsed interlayers has received very little
69 attention compared with hydrated ion exchange, until recent imaging³⁴ and spectroscopic¹⁹
70 studies demonstrated that direct Cs⁺ exchange for K⁺ in phlogopite and illite can occur in the
71 absence of a decollapsed intermediate. Exchange of interlayer K⁺ for Cs⁺ is thermodynamically
72 viable in the presence of aqueous K⁺, since the exchange reaction in mica and collapsed clay
73 interlayers is only weakly selective towards K⁺ (Lammers et al., *in review*).³⁵⁻³⁶ Direct exchange
74 was shown to cause phase separation within individual layers, meaning exchanged layer regions
75 are nearly completely occupied by the exchanging ion (*i.e.* Cs⁺).³⁴ This picture contrasts sharply
76 with the smoothly varying concentration front expected during diffusion-controlled exchange
77 reactions.²⁵ The phase separation of ions within a given layer has long been thought to be
78 thermodynamically favored over mixed interlayer structures, but there is no coherent prevailing
79 view to explain how phase separation occurs in general, and multiple pathways are possible.^{17,37}
80 In addition, direct exchange leads to the formation of interstratified structures,³⁴ where Cs⁺-
81 exchanged layers alternate with layers showing little or no penetration of the exchange front.
82 Interstratification is regularly observed in both anhydrous and swelling clays, for both organic¹⁵⁻
83 ¹⁶ and inorganic^{14, 17, 31, 38} exchanger ions. Cycles of interlayer expansion and collapse driven by
84 exchange with solvated ions (*i.e.* Ca²⁺ or Mg²⁺) followed by K⁺ or Cs⁺ are thought to induce
85 interstratification, because replacement of K⁺ by solvated ions in one layer may strengthen the
86 K⁺ binding in the adjacent layers.^{14, 26, 31-32, 39-40} However, none of the hypothesized pathways can
87 adequately explain formation of interstratified structures during the direct exchange of K⁺ for Cs⁺
88 as observed by Okumura et al.³⁴

89 Here, we use classical molecular dynamics (MD) simulations and density functional
90 theory (DFT) to investigate the mechanism, driving forces and kinetics of direct Cs^+ - K^+
91 exchange in anhydrous interlayers of illite clay minerals. Classical MD simulations are used to
92 identify the types of migration events responsible for interlayer ion exchange and to quantify the
93 distributions in energy barriers associated with these events, and DFT is used to simulate the
94 energy landscape of interlayer ion diffusion in the vicinity of Cs^+ . The combined simulation
95 results provide a detailed understanding of the kinetic phenomena facilitating exchange of Cs^+
96 for K^+ in illite and other micaceous minerals.

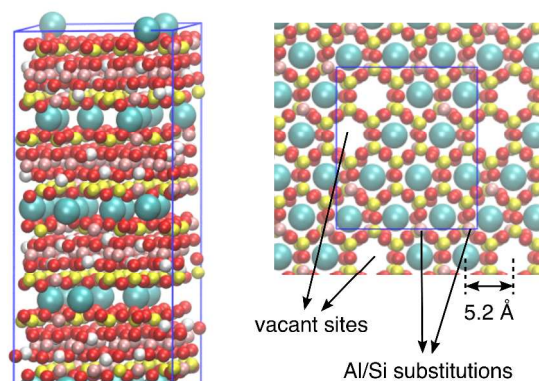
97

98 SIMULATION METHODS

99 We use both classical atomistic molecular dynamics (MD) and density functional theory
100 (DFT) simulations to understand the mechanisms of interlayer ion exchange in illite—ubiquitous
101 in shale formations and known to have an extremely high affinity for Cs^+ . The MD simulations
102 were performed using the simulation package LAMMPS⁴¹ with customized wrappers to perform
103 high-throughput runs. Interatomic interactions between ions and atoms in illite were modeled
104 using the ClayFF potential.⁴² For layered silicates, ClayFF has been shown to faithfully
105 reproduce ion sorption behavior⁴³⁻⁴⁵ and the dynamics of solvated interlayer ions,⁴⁶⁻⁴⁷ but has not
106 been previously tested with respect to ion migration dynamics in anhydrous interlayers. The
107 Climbing Image Nudge Elastic Band (CINEB) method⁴⁸ is employed to quantify the diffusion
108 energy barriers in the interlayer, and harmonic transition state theory to evaluate transport rates
109 based on those barriers.⁴⁹ For the classical MD simulations, we created an atomic model of
110 multilayer illite with the structure determined by Gualtieri⁵⁰ using X-ray powder diffraction
111 combined with Rietveld and reference intensity ratio methods. This 2:1 phyllosilicate is
112 monoclinic with a chemical formula given by $\text{K}_n[\text{Si}_{4-n}\text{Al}_n]\text{Al}_2\text{O}_{10}(\text{OH})_2$, where the square
113 brackets indicate Si and Al located in tetrahedrally coordinated sites in the clay layer, with a
114 fraction n of tetrahedral Si substituted by Al. This isomorphic substitution creates a negative
115 structural charge compensated by K^+ in the interlayer. Our model illite
116 ($\text{K}_{0.7}[\text{Si}_{3.3}\text{Al}_{0.7}]\text{Al}_2\text{O}_{10}(\text{OH})_2$) bears a structural charge of 1.81 mol c/kg, an intermediate value in
117 the non-swelling clays,⁵¹ and contains approximately 30% interlayer site vacancies (Figure 1).
118 The isomorphic substitutions are distributed randomly in the tetrahedral sheet with the

119 restrictions that substitutions cannot occur in neighboring tetrahedral sites.⁵² We optimize the K^+
120 positions for each structure using conjugate gradient potential energy minimization.

121

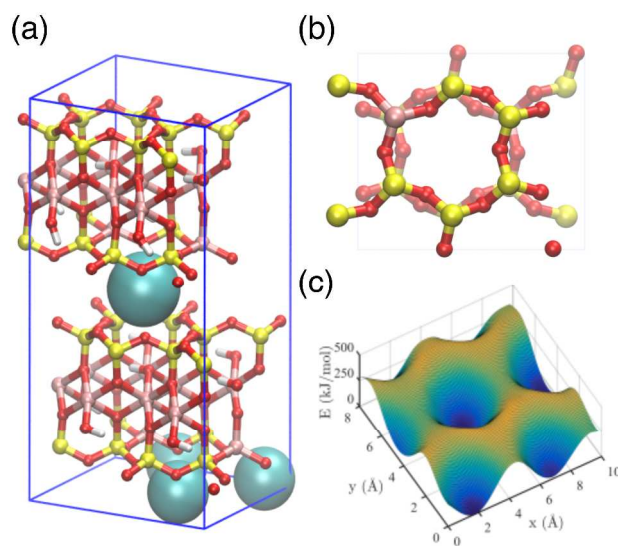


122
123 **Figure 1.** Atomistic illustration of a typical illite structure used in the molecular dynamics simulations in side (left)
124 and plan (right) view. The K^+ (cyan) located in the interlayer regions compensate the structural charge that arises
125 due to Al^{3+} (pink) substitution for Si^{4+} (yellow) in the tetrahedral sheet of the clay layers. Other elements depicted
126 include oxygen (red) and hydrogen (white).
127

128 The DFT simulations are performed at the GGA level of theory with dispersion
129 corrections (revPBE-D3).⁵³⁻⁵⁴ The systems studied contain 164 atoms (Figure 2a) and are
130 composed of two interlayers, one of which is sampled (Figure 2b). Regardless of the number of
131 isomorphic substitutions, the sampled interlayer contains only one ion (K^+ or Cs^+) to facilitate
132 the sampling. The possible excess of negative charge in the sampled interlayer, e.g. if there is
133 more than one isomorphic substitution, is compensated by the addition of K^+ in the other
134 interlayer such that the net charge of the system is neutral overall. The non-sampled interlayer
135 contains K^+ in all cases. In the main text, we show the results for interlayers where $n = 0.75$, the
136 most representative structure for illite, although we also studied cases where $n = 0.25$ and 0.5
137 (Supporting Information, SI). The trends reported for $n = 0.75$ also hold for the other cases. For
138 each value of n , we study 3 distinct scenarios depending on the nature of the ion sampled and the
139 optimized cell dimensions: K^+ in a K^+ -optimized cell (i.e. K^+ in K-illite), Cs^+ in a Cs^+ -optimized
140 cell (i.e. Cs^+ Cs-illite), and K^+ in a Cs^+ -optimized cell (K^+ in Cs-illite).

141 The protocol that we use to reconstruct the potential energy surface (PES) of K^+ and Cs^+
142 in the interlayer from DFT calculations is as follows. First, we optimize the simulation cells with
143 either K^+ or Cs^+ in the sampled interlayer using the Broyden-Fletcher-Goldfarb-Shanno (BFGS)
144 algorithm under triclinic symmetry conditions. Once we have the optimal cell parameters, we

145 generate configurations of the system where the x-y position of the ion in the interlayer is
146 prescribed to a point in a rectangular grid of equispaced points—a total of 378 configurations.
147 For each configuration, the geometry of the system is optimized (with the cell parameters kept
148 constant) and the energy calculated. During the geometry optimization, one Al atom in the
149 octahedral sheet of each layer is constrained, which prevents unphysical translational motions of
150 the layers. The ion is constrained at the prescribed positions in the x-y directions, but it is
151 allowed to relax in the direction perpendicular to the surface. The PES is then reconstructed from
152 the DFT energy data points using a biharmonic interpolation scheme (Figure 2c). Finally, we
153 calculate the minimum energy paths (MEP) connecting the different local minima in the
154 landscape using the zero-temperature string method (ZTS),⁵⁵⁻⁵⁶ which is adequate given the
155 smoothness of the PES. Additional technical details regarding the computational methods are
156 provided in the SI.
157



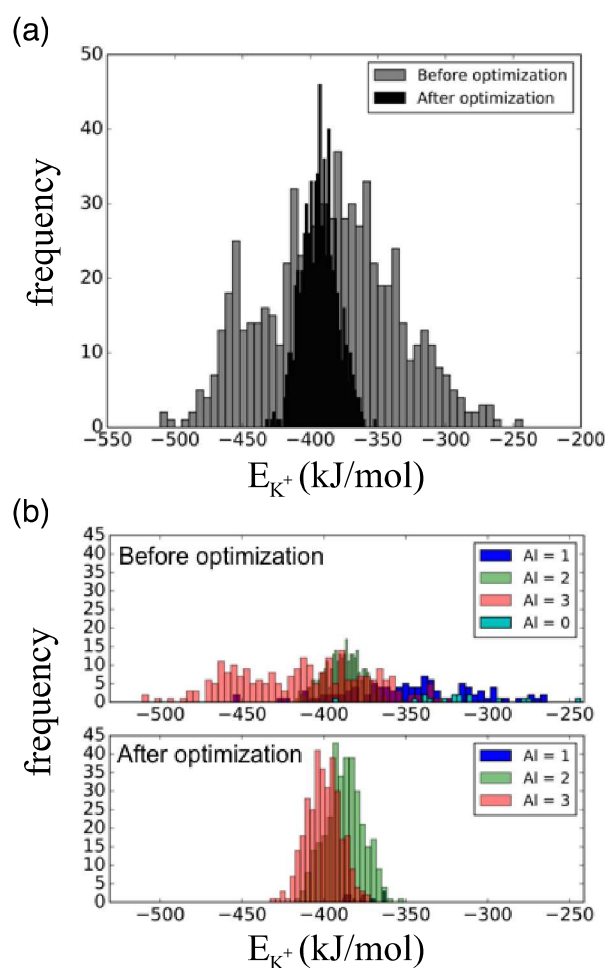
158
159 **Figure 2.** Atomistic illustration of the system used in the DFT simulations. (a) Snapshot of a typical system, where
160 the ions are shown as cyan beads. (b) Plan view of the top and bottom surfaces of the sampled interlayer without the
161 ion. (c) Example of a potential energy surface (PES) reconstructed from DFT energy data.
162

163 RESULTS AND DISCUSSION

164 *Classical Molecular Simulations of Interlayer Energetics and Ion Dynamics*

165 Clay minerals contain vacancies at interlayer sites in inverse proportion to the magnitude
166 of the structural charge. These vacancies facilitate mass transport through the interlayer and are

167 therefore critical to the process of interlayer ion exchange. In order to have a representative
168 system, it is important to optimize the positions of ions and vacancies in the interlayer. Figure 3a
169 shows the distribution of cohesive energies of interlayer cations before (grey) and after (black)
170 optimization of their positions in the interlayer. We find that interlayer K^+ counterions prefer
171 local charge deficit regions adjacent to greater numbers of Si-Al isomorphous substitutions (Figure
172 3b). Thus, layers with locally higher densities of substitutions are likely to contain more
173 counterions and fewer vacancies, indicating that counterion distributions are likely non-
174 random.¹⁰
175



176
177 **Figure 3.** (a) Distribution of cohesive energies of interlayer K^+ before (grey) and after (black) optimization for their
178 positions in the interlayer, (b) distribution of K^+ cohesive energies segmented by the number of Al^{3+} nearest
179 neighbors before and after optimization. The analyses of variance between and within the groups gives F-statistic as
180 234.65 ($p=0$) for $n = 664$, suggesting that the probability that these distributions arise from random, otherwise
181 similar groups, is almost impossible.

182

183 Initially, brute force molecular dynamics (MD) simulations using the ClayFF force field
184 were performed for temperatures between 500-900 K to determine whether interlayer ion
185 migration is observable over nanosecond timescales in K-illite. No migration of the interlayer K^+
186 was observed (SI Figure S1), which suggests that the barrier for migration is too high to directly
187 observe over MD timescales, even at elevated temperatures. Instead, we use the CINEB method
188 to investigate the kinetics of single interlayer ion migration events or hops from occupied to
189 adjacent vacant counterion sites. These elementary steps collectively control the diffusion of
190 interlayer ions and the propagation of ion exchange fronts. CINEB is used to determine the
191 lowest energy path and calculate the energy barriers associated with interlayer ion migration
192 events. Since the local environment around each K^+ is variable—for example, different numbers
193 of neighboring tetrahedral Al and K^+ —we expect there to be a distribution of K^+ migration
194 barriers. In order to capture this distribution, we calculated barriers for an ensemble of several
195 hundred K^+ migrating to all their possible vacant neighboring sites.

196 The green line in Figure 4a shows a typical path followed by a migrating K^+ after
197 optimization of the initial assumed path (black line), in which the K^+ moves past the oxygen ion
198 at the center of the line joining two stable sites. Figure 4b shows a representative migration
199 barrier, where the x-axis reaction coordinate is scaled such that 0 corresponds to one stable site
200 and 1 corresponds to another adjacent, initially vacant, counterion site. In this particular example,
201 the barrier for the forward migration is ~ 250 kJ/mol with the final state ~ 10 kJ/mol higher in
202 energy than the initial state. Figure 4c shows a distribution of migration barriers for over 650
203 cases studied, including reverse migration barriers. For the ground state K-illite structure, we
204 calculate a mean barrier to interlayer ion migration of 226 ± 51 kJ/mol (1σ). Migration events
205 with such large energy barriers cannot be directly observed in conventional MD simulations
206 unless the migration attempt frequencies are orders of magnitude greater than the Einstein
207 frequency (10^{11} – 10^{14} s $^{-1}$), which is typical for single-atom led migrations/transitions in solids.
208 While it is possible for migrations/transitions to have large effective attempt frequencies, such
209 large frequencies are usually only observed for collective processes involving the simultaneous
210 motion of many atoms.⁵⁷

211 The considerable observed variability in the magnitude of the migration barrier requires
212 further discussion. If we assume that the migration path and mechanism itself remains the same
213 for all migration events, we can attribute this variation in part to differences in the cohesive

214 energies of K^+ at stable sites. A simple regression analysis of the data suggests that we can
215 expect about 0.5 kJ/mol increase in barrier for 1 kJ/mol increase in cohesive energy of the stable
216 site (SI Figure S2). These findings demonstrate for the first time a mechanism by which local
217 charge distribution can influence interlayer reaction kinetics. Other potential sources of
218 variability, such as the migration direction (SI Figure S3), have a statistically insignificant
219 impact on the migration barrier. In general, we expect ClayFF to underestimate the true
220 magnitude of the migration barrier, due to the non-bonded nature of the force field that makes
221 structures excessively deformable.⁵⁸⁻⁵⁹

222

223 *Interlayer K^+ Diffusion Dynamics: Comparison with Experiment*

224 Despite the wide range in calculated migration barriers, the values are far too high to
225 explain the amount of exchange observed experimentally, where the exchange front between Cs^+
226 and K^+ is observed to propagate by at least tens of nanometers over 1 year timescales in illite¹⁹
227 and by a similar distance over 24 hour timescales in K-phlogopite.³⁴ This can be shown by
228 simple arguments. Assuming ions diffuse in the interlayer following a random walk, the mean
229 squared displacement (MSD) scales as:

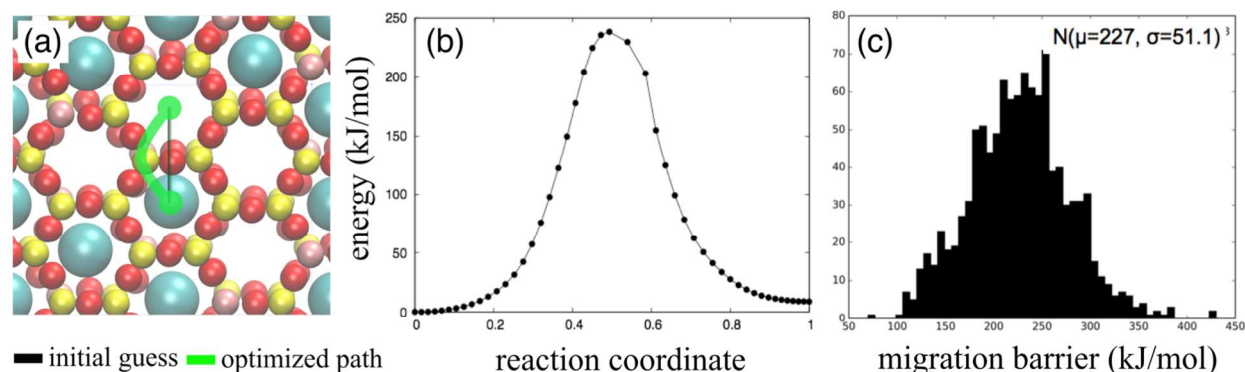
$$230 \quad \langle r^2 \rangle = a^2 N,$$

231 where N is the number of hops and a is the lattice spacing. The value of N depends on elapsed
232 time (t , s) following:

$$233 \quad N = t \times \nu_0 \exp\left(\frac{-E_a}{RT}\right),$$

234 where ν_0 is the frequency of ion vibration in the minima, E_a is the magnitude of the energy
235 barrier for a single hop, R is the gas constant (0.008314 kJ/mol K), and T is absolute temperature
236 (K). For reasonable values of these parameters ($\nu_0 = 10^{13} \text{ s}^{-1}$, $a = 5.2 \text{ \AA}$, $t = 1 \text{ year}$, and $T = 298$
237 K), the CINEB calculated migration barriers correspond to a root MSD of $1.4 \times 10^{-19} \text{ m}$, and a
238 range based on the 1σ uncertainty in the migration barrier of $4.2 \times 10^{-15} \text{ m}$ to $4.9 \times 10^{-21} \text{ m}$.
239 These displacement distances are significantly smaller than even the distances separating stable
240 counterion sites in the illite structure ($5.2 \times 10^{-10} \text{ m}$). Thus, based on these migration barriers, we
241 estimate that the self-diffusion of K^+ in ground state ClayFF illite is far too slow to permit the

242 extent of exchange observed in experiments. In addition, our calculated migration barriers are
 243 significantly higher than values estimated for the diffusion of solvated Na^+ into K-phlogopite,²⁵
 244 which may be limited by the mobility of K^+ at the exchange front. In fact, the largest reported
 245 barrier to hydrated ion exchange with K^+ in mica is ~ 106 kJ/mol,²⁶ significantly less than the
 246 average of our barrier distribution shown in Figure 4c.
 247



248
 249
 250 **Figure 4.** Results a typical CINEB calculation with the optimized ion migration path shown in (a) and its
 251 corresponding energy barrier (b). A histogram summarizing several hundred CINEB results (c) gives a mean energy
 252 barrier of 227 ± 102 kJ/mol (95% of data) for K ion migration from occupied sites to neighboring vacant sites.
 253

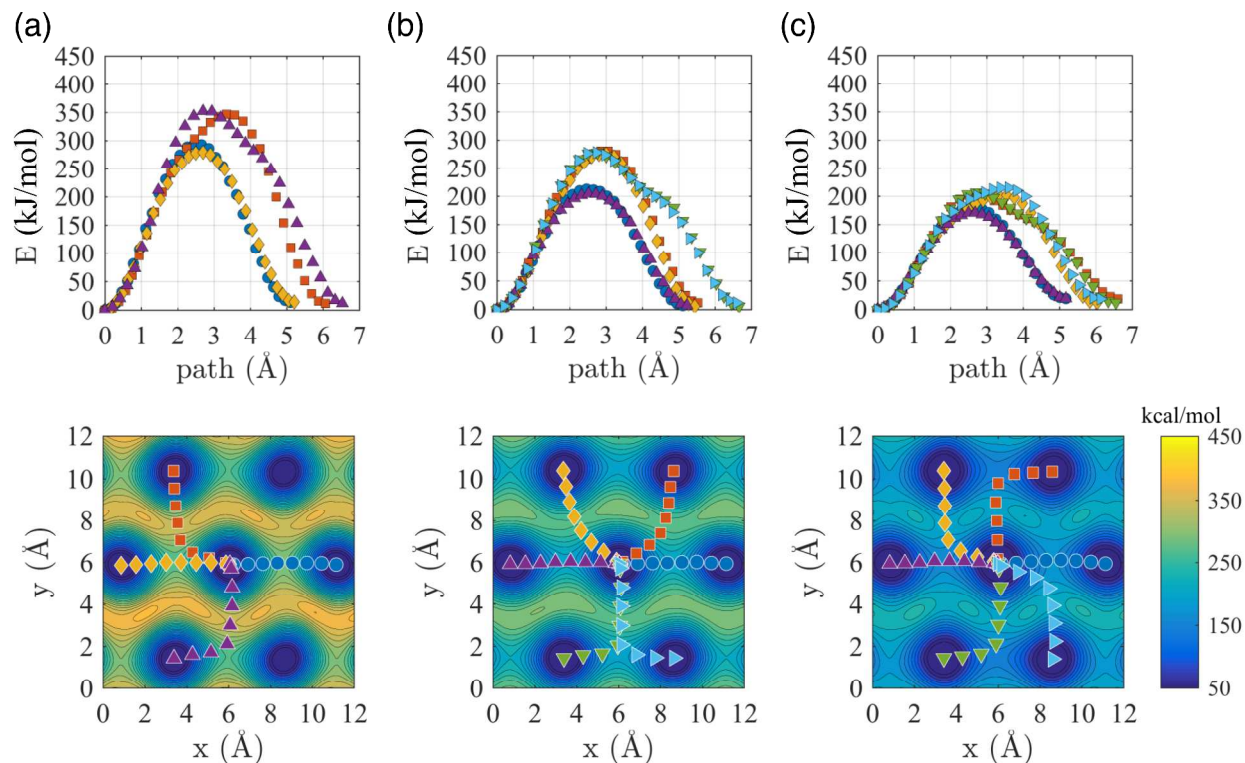
254 *Electronic Structure Calculations of Interlayer Energetics*

255 Given the apparent mismatch with experiments, electronic structure DFT calculations
 256 were performed to verify that the calculated barriers and mechanistic assumptions based on the
 257 ClayFF force field are reasonable. The results are shown for $n = 0.75$ in Figure 5, with additional
 258 results in SI Figures S4 and S5, for $n = 0.25$ and $n = 0.5$ respectively. Overall, the magnitude of
 259 the energy barriers associated with K^+ migration in K-illite (Figure 5a) averaged over all
 260 orientations is 317 ± 36 kJ/mol (1σ), which is approximately 30% higher than the energy barrier
 261 calculated from the CINEB simulations using ClayFF. The DFT simulations show two distinct
 262 pathways of ion migration between occupied and vacant interlayer sites. The first is in agreement
 263 with the CINEB calculations and connects two minima following a curved path that avoids the
 264 oxygen between tetrahedrally coordinated Si or Al (Figure 5a-c). The second pathway is a
 265 straight line between the two minima and occurs only in the horizontal direction (a-axis crystal
 266 orientation). These linear pathways, which ClayFF fails to identify, exhibit substantially lower
 267 energy barriers (by around 40-70 kJ/mol) than the curved paths (Figure 5a-c), suggesting that ion

268 exchange rates in single crystals may be anisotropic. Existing experimental evidence for the
269 exchange front structure is inconclusive: in a recent study, *in situ* imaging of Na⁺-K⁺ exchange in
270 phlogopite appears to show slightly elongated (oval) exchange front structures originating at
271 defects on the scale of a single layer,²⁵ while in an older study, optical imaging gives no evidence
272 of exchange front anisotropy in biotite on the scale of a single crystal.²⁹ Inspection of the clay
273 structure reveals that the Al atoms in the octahedral sheet may be mechanically reinforcing the
274 straight diagonal pathways, forcing the ion to take the alternative curved path (SI Figure S6). The
275 inability of ClayFF to capture this behavior may lay in the fact that it fails to reproduce the
276 ditrigonal geometry of the cavities in the surface of the tetrahedral sheet (SI Figure S7), and also
277 on its inadequate representation of the mechanical properties of layered silicates.⁵⁸⁻⁵⁹ Layer
278 stacking may also influence the occurrence of exchange front anisotropy, which may explain
279 why it can be observed in a single layer but not in a single crystal.

280 Somewhat surprisingly, these calculations show no discernable dependence of the energy
281 barriers on structural charge (Fig. 5 versus SI Figures S4 and S5), which is likely due to the fact
282 that these barriers are controlled by the physical width of the interlayer and thus the size of the
283 counterion. Experiments suggest that exchange of interlayer ions proceeds more rapidly in
284 phases with lower structural charge when driven by a decollapse mechanism,^{12, 30} but these
285 results are not directly comparable to the direct exchange process investigated here. There are no
286 studies to the authors' knowledge investigating the impact of layer charge on rates of ion
287 exchange in anhydrous interlayers. We hypothesize that in the case of interlayers with a large
288 number of interlayer vacancies (i.e. low structural charge), the direct exchange process is likely
289 to be limited by individual migration events, and hence the diffusion energy barriers. However,
290 in the case of interlayers with very high structural charge, where the number of vacancies is
291 minimal, the exchange process will likely be limited instead by the diffusion of vacancies
292 themselves. In this case, exchange rates are expected to be largely independent of the diffusion
293 energy barriers to single ion migration events. This emergent behavior as a function of the
294 interlayer occupancy, or structural charge, merits further research.

295



296
 297 **Figure 5.** Minimum energy paths (MEP) found on the DFT-reconstructed potential energy surfaces (PES). Top-
 298 plots show the energy along the different paths, and bottom-plots show the actual path over the PES. (a) K^+ in K-
 299 illite, (b) Cs^+ in Cs-illite, and (c) K^+ in Cs-illite.

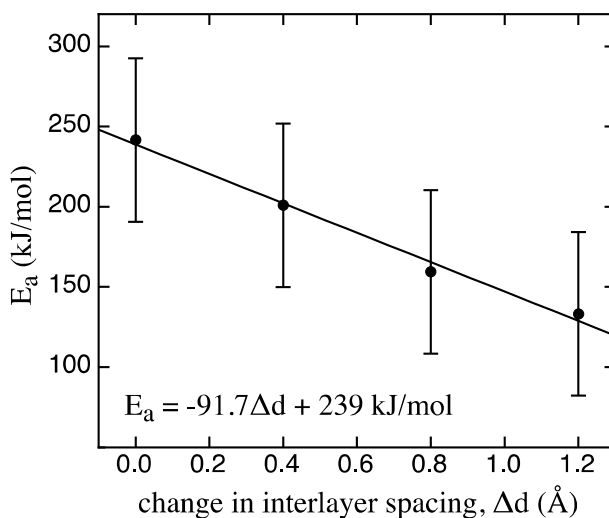
300

301 *Chemical-Mechanical Coupling as a Driver for Exchange*

302 The results of these DFT calculations reinforce our conclusion that the ion migration
 303 barriers of K^+ in ground state K-illite are far too high to explain observed Cs^+ - K^+
 304 exchange dynamics. Thus, an alternative mechanism must be invoked to explain the observed exchange
 305 phenomena. Upon close inspection, we find that the exchange reaction alters the structure of the
 306 interlayer to accommodate the larger size of Cs^+ with respect to K^+ , making the interlayer in the
 307 vicinity of a Cs^+ larger than for K^+ . The ClayFF model predicts a linear increase in the interlayer
 308 spacing with Cs^+ substitution for K^+ (SI Figure S8), and the interlayer spacing of the Cs-illite end
 309 member is $0.67 \pm 0.03 \text{ \AA}$ larger than that of pure K-illite. Similarly, the DFT calculations predict
 310 an increase of the interlayer spacing of 0.75 \AA between K- and Cs-illite end-members, consistent
 311 with measured values.^{19,34} Since the maximum of the energy barrier predicted by both atomistic
 312 and *ab initio* methods is controlled by the position of oxygen atoms that delineate the ditrigonal
 313 cavities, increasing the width of the interlayer region is likely to decrease the magnitude of the
 314 barrier. We hypothesize the existence of a molecular mechanism involving larger exchanging

315 ions, such as Cs^+ , that lowers the migration barrier for K^+ . The increment in interlayer spacing
316 provided by neighboring Cs^+ ions likely reduces the migration barrier for K^+ at the exchange
317 front, leading to a positive-feedback exchange mechanism that accelerates subsequent exchange
318 and migration events.

319 Both DFT and ClayFF CINEB results support this positive feedback hypothesis. Using
320 DFT, we observe that the average energy barrier of K^+ in Cs-illite (Figure 5c)—a realistic
321 scenario for a K^+ ion located at the front of the exchange process, where it has a substantial
322 percentage of Cs^+ neighbors—drops dramatically by 125 kJ/mol (from 317 to 192 kJ/mol).
323 Similarly, the mode of the distribution of activation energy barriers for ion migration calculated
324 using CINEB with ClayFF decreases linearly with increasing Δd (Figure 6). Complete
325 substitution of K^+ by Cs^+ is expected to lower the barrier for K^+ migration at the exchange front
326 to approximately 150 kJ/mol (SI Figure S9). The local increase in interlayer spacing caused by
327 Cs^+ exchange for K^+ lowers the energy barrier for K^+ ion migration, leading to an exponential
328 increase in K^+ diffusivity. According to Equations 1-2, the decrease in barriers predicted by
329 atomistic and *ab initio* simulation results would yield an expected increase in the K^+ ion
330 migration kinetics by 6 and 10 orders of magnitude respectively. These results provide evidence
331 of a new mechanism for direct exchange of anhydrous ions that arises from the interplay between
332 interlayer structure and reactivity (*i.e.*, “chemical-mechanical coupling”) and that does not
333 require intermediate swelling states (decollapse) to occur.



334

335

336 **Figure 6.** The magnitude of the K^+ migration barrier decreases linearly with increasing interlayer spacing, from the
337 K-illite end-member ($\Delta d = 0$ Å) to layer spacings typical of the Cs-illite end-member ($\Delta d = 0.67 \pm 0.03$ Å).

338 *Formation of Phase-Separated Interlayers*

339 Experimental observations of the structure of the exchange front show that it is sharp,
340 instead of a smooth, diffusive interface, and that the Cs⁺ substituted region is almost completely
341 clear of K⁺.³⁴ The positive-feedback exchange mechanism proposed here explains why a sharp
342 front will facilitate K⁺ exchange (*i.e.* K⁺ is only highly mobile in the vicinity of Cs⁺) but does not
343 fully elucidate the near-complete exchange that is observed. To explain this behavior, we
344 evaluated the thermodynamic driving force for Cs- and K-illite phase separation by calculating
345 the change in free energy as a function of the mole fraction of Cs⁺ randomly mixed in the
346 interlayer. Based on an ensemble of ClayFF energy minimization calculations, we find that there
347 is a significant energetic penalty for mixing small amounts of Cs⁺ in K-illite interlayers and vice
348 versa (SI Figure 10). For example, replacing 10% of the K⁺ by Cs⁺ results in a per-molar free
349 energy penalty of 13.2 ± 6.0 kJ/mol. Thus, the de-mixing of Cs⁺ and K⁺ in the interlayer is
350 strongly favored. We conclude that both the bulk phase thermodynamics and the kinetic
351 feedbacks associated with Cs⁺-K⁺ exchange lead to the formation of phase-separated interlayer
352 regions. Thermodynamically favorable phase-separated domains naturally arise even in the
353 absence of a heterogeneous layer charge distribution, which has long been invoked to explain the
354 prevalence of these structures in clays.⁶⁰

355

356 *Additional Factors Influencing Interlayer Exchange Kinetics*

357 Despite some quantitative discrepancies between DFT and ClayFF, both methods capture
358 the trend that supports our hypothesized molecular mechanism for promoting the K⁺/Cs⁺
359 exchange. It is worth noticing that the energy barriers reported here refer to potential energy, and
360 although we do not expect entropy to play a major role in the process due to the large binding
361 energies involved, it is important to keep in mind that these are upper limits to the real free
362 energy barriers. While it is possible that the presence of trace interlayer water or structural
363 defects could accelerate K⁺ migration, it is not necessary to invoke these phenomena to explain
364 the observed direct exchange dynamics. The feedback between interlayer structure and exchange
365 kinetics—chemical-mechanical coupling—is sufficient to explain the direct exchange of Cs⁺ for
366 K⁺ in micaceous minerals.

367

368 Additional geochemical factors such as the composition of the aqueous solution and the
369 structure and protonation state of the edge will play a role in mediating the macroscopic kinetics
370 of the exchange reaction, but these are unlikely to alter the basic molecular mechanism driving
371 the exchange. Formation of interstratified structures in which substituted layers randomly
372 alternate with pristine layers may arise as a consequence of mechanical interactions between
373 layers, which promote exchange in some layers at the expense of others, and the dynamics of this
374 process will be the focus of a future study.

375

376 *Environmental Significance*

377 The accessibility of interlayer sites to exchange implies that the ion exchange capacity of
378 non-swelling clays, those that have an extremely high affinity for radiocesium, may be
379 significantly greater than expected based on standard short-term (often 24 hour) exchange
380 experiments. It is likely that ions of similar size and charge to K^+ , also including NH_4^+ , can
381 undergo direct exchange with micaceous clay interlayers in the absence of an expanded
382 intermediate. Indeed, redox gradients in the environment can generate high concentrations of
383 NH_4^+ in pore fluids, which in turn can remobilize illite-bound radiocesium.⁶¹ The contribution of
384 the clay interlayer specifically to such ion exchange driven remobilization has not been
385 established.

386 In addition to their role in regulating radiocesium transport, non-swelling clay minerals
387 control the availability of critical soil nutrients, K^+ and NH_4^+ .^{24, 27, 62} Given the slight
388 thermodynamic preference of the interlayer for K^+ relative to species of like size and charge,
389 direct exchange reactions can proceed even in the presence of aqueous K^+ , which is known to
390 inhibit interlayer ion exchange in the swelling clays.^{28, 63} Thus, we expect the long-term transport
391 behavior of these species in the environment to be controlled at least in part by exchange
392 reactions involving micaceous clay interlayers. Because these phases dominate the clay mineral
393 fraction of sedimentary rocks globally, collapsed interlayers may in fact constitute a reservoir of
394 ion exchange capacity that has been largely overlooked. Direct anhydrous interlayer ion
395 exchange could play a significant role in regulating the mass transport of nutrients and
396 radionuclides in the environment and thus merits further study.

397

398

399 **ASSOCIATED CONTENT**400 **Supporting Information**

401 This material is available free of charge via the Internet at <http://pubs.acs.org/>. It contains
402 additional details regarding the simulation methods employed, the calculation of the exchange
403 thermodynamics, and nine figures corresponding to further analysis mentioned in the main text.

404

405 **AUTHOR INFORMATION**406 **Corresponding Author**

407 Email lnlammers@berkeley.edu

408 **Notes**

409 The authors declare no competing financial interest.

410

411 **ACKNOWLEDGEMENTS**

412 The Laboratory Directed Research and Development Program of Lawrence Berkeley National
413 Laboratory supported this work under U.S. Department of Energy Contract No. DE-AC02-
414 05CH11231. This research used resources of the National Energy Research Scientific Computing
415 Center, a DOE Office of Science User Facility supported by the Office of Science of the U.S.
416 Department of Energy under Contract No. DE-AC02-05CH11231.

417

418 **REFERENCES**

- 419 1. Evans, D. W.; Alberts, J. J.; Clark, R. A., Reversible ion-exchange fixation of cesium-
420 137 leading to mobilization from reservoir sediments. *Geochimica et Cosmochimica Acta* **1983**,
421 *47* (6), 1041-1049.
- 422 2. Anderson, S. J.; Sposito, G., Cesium-Adsorption Method for Measuring Accessible
423 Structural Surface Charge. *Soil Science Society of America Journal* **1991**, *55* (6), 1569-1576.
- 424 3. Hinton, T. G.; Kaplan, D. I.; Knox, A. S.; Coughlin, D. P.; Nascimento, R. V.; Watson, S.
425 I.; Fletcher, D. E.; Koo, B.-J., Use of illite clay for in situ remediation of ¹³⁷Cs-contaminated
426 water bodies: field demonstration of reduced biological uptake. *Environmental Science &*
427 *Technology* **2006**, *40* (14), 4500-4505.

- 428 4. Bourg, I.; Sposito, G., Ion exchange phenomena. In *Handbook of Soil Science, Properties,*
429 *and Processes, 2nd Ed.*, Huang, P.; Li, Y.; Sumner, M., Eds. CRC Press: 2011.
- 430 5. Tachi, Y.; Yotsuji, K.; Seida, Y.; Yui, M., Diffusion and sorption of Cs⁺, I⁻ and HTO in
431 samples of the argillaceous Wakkanai Formation from the Horonobe URL, Japan: Clay-based
432 modeling approach. *Geochimica et Cosmochimica Acta* **2011**, *75* (22), 6742-6759.
- 433 6. Gaboreau, S.; Claret, F.; Crouzet, C.; Giffaut, E.; Tournassat, C., Caesium uptake by
434 Callovian–Oxfordian clayrock under alkaline perturbation. *Applied Geochemistry* **2012**, *27* (6),
435 1194-1201.
- 436 7. Chen, Z.; Montavon, G.; Ribet, S.; Guo, Z.; Robinet, J.; David, K.; Tournassat, C.;
437 Grambow, B.; Landesman, C., Key factors to understand in-situ behavior of Cs in Callovo–
438 Oxfordian clay-rock (France). *Chemical Geology* **2014**, *387*, 47-58.
- 439 8. Fan, Q.; Tanaka, M.; Tanaka, K.; Sakaguchi, A.; Takahashi, Y., An EXAFS study on the
440 effects of natural organic matter and the expandability of clay minerals on cesium adsorption and
441 mobility. *Geochimica et Cosmochimica Acta* **2014**, *135*, 49-65.
- 442 9. Mukai, H.; Hatta, T.; Kitazawa, H.; Yamada, H.; Yaita, T.; Kogure, T., Speciation of
443 radioactive soil particles in the Fukushima contaminated area by IP autoradiography and
444 microanalyses. *Environmental Science & Technology* **2014**, *48* (22), 13053-13059.
- 445 10. Ngouana W, B. F.; Kalinichev, A. G., Structural arrangements of isomorphous
446 substitutions in smectites: Molecular simulation of the swelling properties, interlayer structure,
447 and dynamics of hydrated Cs–montmorillonite revisited with new clay models. *The Journal of*
448 *Physical Chemistry C* **2014**, *118* (24), 12758-12773.
- 449 11. Loganathan, N.; Yazaydin, A. O.; Bowers, G. M.; Kalinichev, A. G.; Kirkpatrick, R. J.,
450 Structure, Energetics, and Dynamics of Cs⁺ and H₂O in Hectorite: Molecular Dynamics
451 Simulations with an Unconstrained Substrate Surface. *The Journal of Physical Chemistry C* **2016**,
452 *120* (19), 10298-10310.

- 453 12. Scott, A.; Smith, S., Susceptibility of interlayer potassium in micas to exchange with
454 sodium. In *Clays and Clay Minerals: Proceedings of the Fourteenth National Conference*,
455 *Berkeley, California*, Elsevier: 1966; pp 69-80.
- 456 13. Reichenbach, H.; Rich, C., Potassium release from muscovite as influenced by particle
457 size. *Clays and Clay Minerals* **1969**, *17*, 23-29.
- 458 14. Sawhney, B., Selective sorption and fixation of cations by clay minerals: a review. *Clays*
459 *and Clay Minerals* **1972**, *20* (9), 93-100.
- 460 15. Barrer, R.; Brummer, K., Relations between partial ion exchange and interlamellar
461 sorption in alkylammonium montmorillonites. *Transactions of the Faraday Society* **1963**, *59*,
462 959-968.
- 463 16. Theng, B.; Greenland, D.; Quirk, J., Adsorption of alkylammonium cations by
464 montmorillonite. *Clay Minerals* **1967**, *7* (1), 1-17.
- 465 17. Nadeau, P.; Wilson, M.; McHardy, W.; Tait, J., Interstratified clays as fundamental
466 particles. *Science* **1984**, *225*, 923-925.
- 467 18. Suter, J. L.; Groen, D.; Coveney, P. V., Mechanism of Exfoliation and Prediction of
468 Materials Properties of Clay–Polymer Nanocomposites from Multiscale Modeling. *Nano letters*
469 **2015**, *15* (12), 8108-8113.
- 470 19. Fuller, A. J.; Shaw, S.; Ward, M. B.; Haigh, S. J.; Mosselmanns, J. F. W.; Peacock, C. L.;
471 Stackhouse, S.; Dent, A. J.; Trivedi, D.; Burke, I. T., Caesium incorporation and retention in
472 illite interlayers. *Applied Clay Science* **2015**, *108*, 128-134.
- 473 20. Poinssot, C.; Baeyens, B.; Bradbury, M. H., Experimental and modelling studies of
474 caesium sorption on illite. *Geochimica et Cosmochimica Acta* **1999**, *63* (19–20), 3217-3227.
- 475 21. Benedicto, A.; Missana, T.; Fernández, A. M., Interlayer collapse affects on cesium
476 adsorption onto illite. *Environmental science & technology* **2014**, *48* (9), 4909-4915.

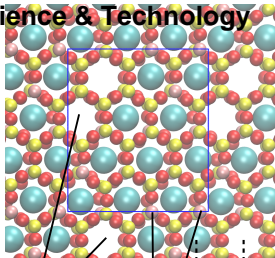
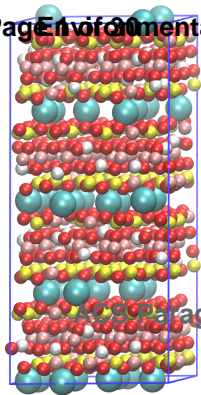
- 477 22. Tamura, K.; Kogure, T.; Watanabe, Y.; Nagai, C.; Yamada, H., Uptake of Cesium and
478 Strontium Ions by Artificially Altered Phlogopite. *Environmental Science & Technology* **2014**,
479 48 (10), 5808-5815.
- 480 23. Wauters, J.; Sweeck, L.; Valcke, E.; Elsen, A.; Cremers, A., Availability of radiocaesium
481 in soils: a new methodology. *Science of the Total Environment* **1994**, 157, 239-248.
- 482 24. Barshad, I., Cation exchange in micaceous minerals: II. Replaceability of ammonium and
483 potassium from vermiculite, biotite, and montmorillonite. *Soil Science* **1954**, 78 (1), 57-76.
- 484 25. Sánchez-Pastor, N.; Aldushin, K.; Jordan, G.; Schmahl, W. W., K⁺-Na⁺ exchange in
485 phlogopite on the scale of a single layer. *Geochimica et Cosmochimica Acta* **2010**, 74 (7), 1954-
486 1962.
- 487 26. Rausell-Colom, J.; Sweatman, T.; Wells, C.; Norrish, K., Studies in the artificial
488 weathering of mica. *Experimental Pedology* **1965**, 40-72.
- 489 27. Quirk, J.; Chute, J., Potassium release from mica-like clay minerals. In *9th International*
490 *Congress of Soil Science Transactions*, Holmes, J. W., Ed. International Society of Soil Science:
491 Adelaide, Australia, 1968; Vol. 2, pp 671-681.
- 492 28. Reichenbach, H.; Rich, C., Preparation of dioctahedral vermiculites from muscovite and
493 subsequent exchange properties. In *9th International Congress of Soil Science Transactions*,
494 Holmes, J. W., Ed. International Society of Soil Science: 1968; Vol. 1, pp 709-719.
- 495 29. Scott, A., Effect of particle size on interlayer potassium exchange in micas. In *9th*
496 *International Congress of Soil Science Transactions*, Holmes, J. W., Ed. International Society of
497 Soil Science: Adelaide, Australia, 1968; Vol. 2, pp 649-658.
- 498 30. Lai, T.; Mortland, M., Diffusion of ions in bentonite and vermiculite. *Soil Science Society*
499 *of America Journal* **1961**, 25 (5), 353-357.
- 500 31. Sawhney, B., Interstratification in vermiculite. *Clays and Clay Minerals* **1967**, 15, 75-84.

- 501 32. Sawhney, B., Regularity of interstratification as affected by charge density in layer
502 silicates. *Soil Science Society of America Journal* **1969**, *33* (1), 42-46.
- 503 33. Scott, A.; Hunziker, R.; Hanway, J., Chemical extraction of potassium from soils and
504 micaceous minerals with solutions containing sodium tetraphenylboron. I. Preliminary
505 experiments. *Soil Science Society of America Journal* **1960**, *24* (3), 191-194.
- 506 34. Okumura, T.; Tamura, K.; Fujii, E.; Yamada, H.; Kogure, T., Direct observation of
507 cesium at the interlayer region in phlogopite mica. *Microscopy* **2014**, *63* (1), 65-72.
- 508 35. Okumura, M.; Nakamura, H.; Machida, M., Mechanism of strong affinity of clay
509 minerals to radioactive cesium: first-principles calculation study for adsorption of cesium at
510 frayed edge sites in muscovite. *Journal of the Physical Society of Japan* **2013**, *82* (3), 033802.
- 511 36. Suehara, S.; Yamada, H., Cesium stability in a typical mica structure in dry and wet
512 environments from first-principles. *Geochimica et Cosmochimica Acta* **2013**, *109*, 62-73.
- 513 37. Xu, S.; Boyd, S. A., Cation exchange chemistry of hexadecyltrimethylammonium in a
514 subsoil containing vermiculite. *Soil Science Society of America Journal* **1994**, *58* (5), 1382-1391.
- 515 38. Kogure, T.; Morimoto, K.; Tamura, K.; Sato, H.; Yamagishi, A., XRD and HRTEM
516 evidence for fixation of cesium ions in vermiculite clay. *Chemistry Letters* **2012**, *41* (4), 380-382.
- 517 39. Bassett, W. A., The origin of the vermiculite deposit at Libby, Montana. *American*
518 *Mineralogist* **1959**, *44* (3-4), 282-299.
- 519 40. Farmer, V.; Wilson, M., Experimental conversion of biotite to hydrobiotite. *Nature* **1970**,
520 *226*, 841.
- 521 41. Plimpton, S., Fast parallel algorithms for short-range molecular dynamics. *Journal of*
522 *Computational Physics* **1995**, *117* (1), 1-19.
- 523 42. Cygan, R. T.; Liang, J.-J.; Kalinichev, A. G., Molecular models of hydroxide,
524 oxyhydroxide, and clay phases and the development of a general force field. *The Journal of*
525 *Physical Chemistry B* **2004**, *108* (4), 1255-1266.

- 526 43. Bourg, I. C.; Sposito, G., Connecting the molecular scale to the continuum scale for
527 diffusion processes in smectite-rich porous media. *Environmental Science & Technology* **2010**,
528 *44* (6), 2085-2091.
- 529 44. Ferrage, E.; Sakharov, B. A.; Michot, L. J.; Delville, A.; Bauer, A.; Lanson, B.; Grangeon,
530 S.; Frapper, G.; Jiménez-Ruiz, M.; Cuello, G. J., Hydration Properties and Interlayer
531 Organization of Water and Ions in Synthetic Na-Smectite with Tetrahedral Layer Charge. Part 2.
532 Toward a Precise Coupling between Molecular Simulations and Diffraction Data. *The Journal of*
533 *Physical Chemistry C* **2011**, *115* (5), 1867-1881.
- 534 45. Marry, V.; Dubois, E.; Malikova, N.; Durand-Vidal, S.; Longeville, S.; Breu, J., Water
535 dynamics in hectorite clays: Influence of temperature studied by coupling neutron spin echo and
536 molecular dynamics. *Environmental Science & Technology* **2011**, *45* (7), 2850-2855.
- 537 46. Holmboe, M.; Bourg, I. C., Molecular dynamics simulations of water and sodium
538 diffusion in smectite interlayer nanopores as a function of pore size and temperature. *The*
539 *Journal of Physical Chemistry C* **2013**, *118* (2), 1001-1013.
- 540 47. Tertre, E.; Delville, A.; Prêt, D.; Hubert, F.; Ferrage, E., Cation diffusion in the interlayer
541 space of swelling clay minerals—A combined macroscopic and microscopic study. *Geochimica et*
542 *Cosmochimica Acta* **2015**, *149*, 251-267.
- 543 48. Henkelman, G.; Uberuaga, B. P.; Jónsson, H., A climbing image nudged elastic band
544 method for finding saddle points and minimum energy paths. *The Journal of Chemical Physics*
545 **2000**, *113* (22), 9901-9904.
- 546 49. Vineyard, G. H., Frequency factors and isotope effects in solid state rate processes.
547 *Journal of Physics and Chemistry of Solids* **1957**, *3* (1-2), 121-127.
- 548 50. Gualtieri, A. F., Accuracy of XRPD QPA using the combined Rietveld–RIR method.
549 *Journal of Applied Crystallography* **2000**, *33* (2), 267-278.
- 550 51. Sposito, G., *The Chemistry of Soils*. Oxford university press: 2008.

- 551 52. Sainz-Diaz, C.; Cuadros, J.; Hernández-Laguna, A., Analysis of cation distribution in the
552 octahedral sheet of dioctahedral 2: 1 phyllosilicates by using inverse Monte Carlo methods.
553 *Physics and Chemistry of Minerals* **2001**, 28 (7), 445-454.
- 554 53. Grimme, S.; Antony, J.; Ehrlich, S.; Krieg, H., A consistent and accurate ab initio
555 parametrization of density functional dispersion correction (DFT-D) for the 94 elements H-Pu.
556 *The Journal of Chemical Physics* **2010**, 132 (15), 154104.
- 557 54. Zhang, Y.; Yang, W., Comment on “Generalized gradient approximation made simple”.
558 *Physical Review Letters* **1998**, 80 (4), 890.
- 559 55. Weinan, E.; Ren, W.; Vanden-Eijnden, E., Simplified and improved string method for
560 computing the minimum energy paths in barrier-crossing events. *The Journal of Chemical*
561 *Physics* **2007**, 126 (16), 164103.
- 562 56. Weinan, E.; Ren, W.; Vanden-Eijnden, E., String method for the study of rare events.
563 *Physical Review B* **2002**, 66 (5), 052301.
- 564 57. Uberuaga, B.; Hoagland, R.; Voter, A.; Valone, S., Direct transformation of vacancy
565 voids to stacking fault tetrahedra. *Physical Review Letters* **2007**, 99 (13), 135501.
- 566 58. Shahsavari, R.; Pellenq, R. J.-M.; Ulm, F.-J., Empirical force fields for complex hydrated
567 calcio-silicate layered materials. *Physical Chemistry Chemical Physics* **2011**, 13 (3), 1002-1011.
- 568 59. Teich-McGoldrick, S. L.; Greathouse, J. A.; Cygan, R. T., Molecular dynamics
569 simulations of structural and mechanical properties of muscovite: pressure and temperature
570 effects. *The Journal of Physical Chemistry C* **2012**, 116 (28), 15099-15107.
- 571 60. Vali, H.; Koster, H., Expanding behaviour, structural disorder, regular and random
572 irregular interstratification of 2:1 layer-silicates studied by high-resolution images of
573 transmission electron microscopy. *Clay Minerals* **1986**, 21 (5), 827-859.
- 574 61. Comans, R. N. J.; Middelburg, J. J.; Zonderhuis, J.; Woittiez, J. R. W.; Lange, G. J. D.;
575 Das, H. A.; Weijden, C. H. V. D., Mobilization of radiocaesium in pore water of lake sediments.
576 *Nature* **1989**, 339 (6223), 367-369.

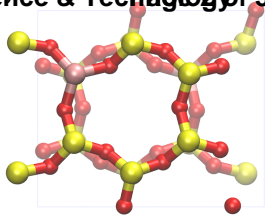
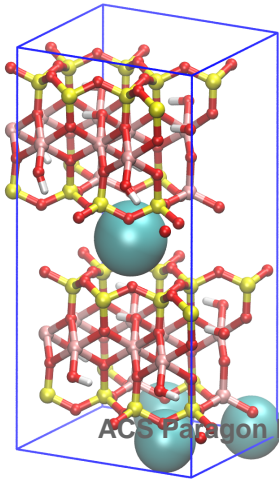
- 577 62. Smith, S. J.; Clark, L. J.; Scott, A. D., Exchangeability of potassium in soils. In *9th*
578 *International Congress of Soil Science Transactions*, Holmes, J. W., Ed. International Society of
579 Soil Science: Adelaide, Australia, 1968; Vol. 2, pp 661-670.
- 580 63. Boek, E. S.; Coveney, P. V.; Skipper, N. T., Monte Carlo molecular modeling studies of
581 hydrated Li-, Na-, and K-smectites: Understanding the role of potassium as a clay swelling
582 inhibitor. *Journal of the American Chemical Society* **1995**, *117* (50), 12608-12617.
583



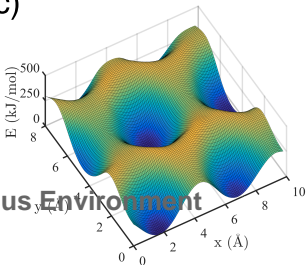
vacant sites

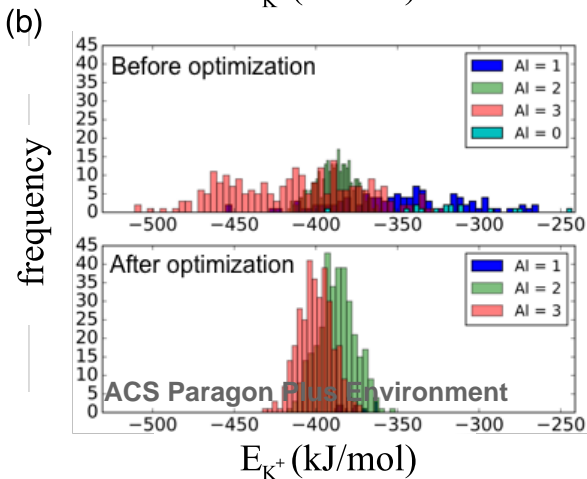
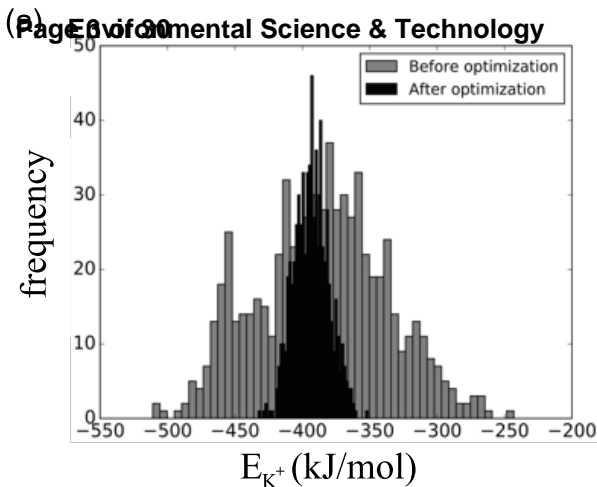
Al/Si substitutions

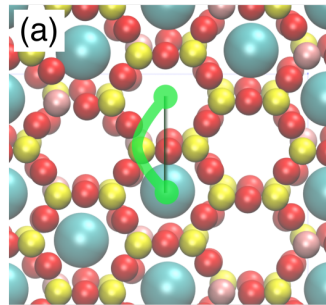
5.2 Å



(c)







■ initial guess ■ optimized path

